# Transferable force-constant modeling of vibrational thermodynamic properties in fcc-based Al-*TM* (*TM*=Ti, Zr, Hf) alloys

Jefferson Z. Liu* and G. Ghosh
*Department of Materials Science and Engineering, Northwestern University, Evanston, Illinois 60208, USA*

A. van de Walle
*Engineering & Applied Science Division, California Institute of Technology, Pasadena, California 91125, USA*

M. Asta
*Department of Chemical Engineering and Materials Science, University of California at Davis, Davis, California 95616, USA*
(Received 26 July 2006; revised manuscript received 6 December 2006; published 28 March 2007)

The vibrational thermodynamic properties of ordered and disordered fcc-based alloys in three aluminum transition-metal (*TM*) systems, Al-*TM* (*TM*=Ti, Zr, and Hf), are computed by first principles methods employing supercell calculations and the transferable-force-constant (TFC) approach. In order to obtain accurate values for the high-temperature limit of the vibrational mixing entropies in these systems, it is necessary to parametrize the dependence of the force constants on both the equilibrium bond length and the *TM* concentration in the TFC method. Provided this concentration dependence is accounted for, the TFC approach is shown to lead to predictions for the vibrational mixing entropy accurate to within approximately 20%. The utility of the TFC method is demonstrated by its application to the calculation of vibrational entropies of mixing for approximately 30 structures in each of the three Al-*TM* systems, facilitating the construction of well converged vibrational-entropy cluster expansions. The calculations yield large and negative values for the vibrational mixing entropies of both ordered and disordered alloys, with an overall magnitude of up to $1.0k_B$/atom, and ordering entropies (i.e., the difference between the vibrational entropy of ordered and disordered phases at the same composition) in the range of $0.2-0.3k_B$/atom for concentrated alloys. Calculated results are shown to be in good agreement with experimental data available for the Al-Ti system.

DOI: 10.1103/PhysRevB.75.104117 PACS number(s): 61.66.Dk, 65.40.Gr

## I. INTRODUCTION

While it has long been appreciated that vibrational entropy ($S_{\mathrm{vib}}$) plays a primary role in governing the relative finite-temperature stability of crystalline structures with different coordination numbers (e.g., fcc versus bcc), the effects of phonons on the phase stability of substitutional alloys, with a common underlying parent lattice, was elucidated only relatively recently. Over the past decade, detailed experimental work based on calorimetry and neutron scattering[1–11] has yielded measured values for vibrational-entropy differences between ordered and disordered substitutional alloy phases with magnitudes on the order of $0.1-0.2k_B$/atom. These ordering entropies are significant relative to the maximum value of the configurational entropy, $0.69k_B$/atom. The experimental findings have motivated a number of theoretical investigations (for a recent review, see Ref. 12) which have confirmed the large magnitudes of the vibrational contribution to the free-energy difference between ordered and disordered phases in several metallic-alloy systems.[13,14] In addition, recent theoretical studies have demonstrated pronounced effects of vibrational entropy on calculated solvus boundaries for Al-based alloy systems.[15–17] These findings demonstrating that vibrational entropy can have appreciable effects on phase-boundary temperatures have motivated a number of recent efforts aimed at developing computationally efficient methods for calculating $S_{\mathrm{vib}}$ for ordered and disordered phases within the context of first-principles calculations of alloy phase diagrams.

In principle, the cluster expansion framework,[18] which has been extensively developed to model alloy configurational energetics (e.g., Ref. 19), can be readily extended as a method for calculating $S_{\mathrm{vib}}$ in ordered and disordered substitutional alloy phases. This approach involves the calculation of vibrational entropies for a number of ordered atomic configurations, from which the interaction parameters in a cluster expansion of $S_{\mathrm{vib}}$ can be readily derived through the so-called structure-inversion approach.[20,21] Once the vibrational-entropy cluster expansion coefficients have been parametrized, the magnitude of $S_{\mathrm{vib}}$ for any ordered or disordered phase can be readily calculated from a knowledge of the equilibrium values of the multisite cluster correlation functions derived, for example, from Monte Carlo simulations. Under the assumption of harmonic lattice vibrations,[22–24] the knowledge of phonon densities of states (DOS) for a given crystal structure is sufficient to determine its vibrational entropy. While obtaining the phonon DOS for a given ordered structure is by now a relatively routine task with modern first-principles electronic-structure codes, this process has to be repeated for many configurations (about twenty to thirty) in order to properly fit a cluster expansion, making the overall procedure relatively computationally demanding.

One method that has been proposed to alleviate this problem is to transfer force constants, for a given chemical bond type, between different chemical environments. Currently, most of the work in calculating $S_{\mathrm{vib}}$ is associated with the numerical determination of the force constants. The ability to

 

transfer force constants between different ordered alloy structures can thus result in a significant time savings in the construction of a cluster expansion for $S_{\mathrm{vib}}$. The approach of transferring force constants between different atomic configurations has been used in the $Ni_3Al$ system,[25] Al-Li,[26] oxides,[27] and semiconductors.[28] In the Al-Li system, an approach for transferring force constants was introduced which reproduced the elastic constants reasonably well (with about a 10% relative error), although relatively large errors were found for calculations of the vibrational entropy. Recently van de Walle *et al.*[12,29,30] observed, in first-principles calculations of $S_{\mathrm{vib}}$ in the Ni-Al and Pd-V systems, that the magnitudes of the force constants are strongly correlated with the corresponding bond lengths and, as a result, that the force constant versus bond length relationships exhibit better transferability than the force constants themselves. This offers an opportunity for considerable computational savings in the construction of a cluster expansion, since the force constant versus bond length relationships can be determined from a relatively small number of first-principles calculations for a few select configurations, and can then be used to rapidly determine the force constants for many other atomic configurations where the equilibrium bond lengths are a by-product of a fully relaxed calculation of its formation energy. This transferable force-constant (TFC) approach was shown to yield calculated values for $S_{\mathrm{vib}}$ with an error less than about $0.02-0.05k_B$/atom in the Pd-V and Ni-Al systems. Similar results were also obtained more recently by Wu *et al.*[31] in their systematic study of vibrational thermodynamic properties of late-transition and noble-metal alloy systems.

In this paper we examine the applicability of the TFC method in the calculation of vibrational entropies for fcc-based phases in the three aluminum transition-metal (*TM*) systems, Al-*TM* (*TM*=Ti, Zr, and Hf). Due to the technological interest in these materials, phase stability in each system has been the subject of a large number of previous experimental and theoretical investigations (for a recent review see Ref. 32). Despite this large amount of work, the magnitudes of the vibrational contributions to the thermodynamic properties of these alloys have not been calculated to date, and estimates based on thermodynamic measurements are available only for the Al-Ti system. Of particular interest in the current work is the calculation of the magnitudes of the vibrational entropies of mixing for both ordered and disordered alloy phases. For this purpose we employ the cluster-expansion framework based on calculations of $S_{\mathrm{vib}}$, performed within the TFC approach. We find that in order to obtain accurate values of $S_{\mathrm{vib}}$ with this approach, it is essential that the dependence of the magnitudes of the force constants on the *TM* concentration is accounted for, in addition to the bond length. The pronounced composition dependencies of the calculated force constants in Al-*TM* (*TM*=Ti, Zr, and Hf) systems is a feature that has not been previously observed in applications of the TFC method to studies of vibrational thermodynamic properties in substitutional alloys. The origin of this effect in the Al-*TM* alloys considered here is likely a consequence of the pronounced charge-transfer effects associated with the bonding in these systems. Provided that the concentration dependencies are accounted for, the TFC method is found to yield calculated values of the mixing entropy accurate to within approximately 20%. With the TFC approach, vibrational entropies are calculated for roughly 30 structures in each of the three Al-*TM* systems, enabling the derivation of well-converged cluster expansions for $S_{\mathrm{vib}}$. The magnitudes of the vibrational mixing entropies for ordered and disordered alloy configurations are calculated to be large and negative, with magnitudes (for ordered alloys) as large as $1.0k_B$/atom. The vibrational entropy of ordering (defined as the difference in $S_{\mathrm{vib}}$ between ordered and disordered alloys with the same composition and parent lattice) is calculated to be on the order of $0.2-0.3k_B$/atom for concentrated alloy compositions.

## II. METHODOLOGY

Under the approximation of harmonic lattice vibrations, and in the high temperature limit, the vibrational entropy (per atom) can be written as a logarithmic moment of the phonon DOS $g(\omega)$:[22,23]

$$S_{\mathrm{vib}} = k_B\left[3 - \int_0^\infty \ln\left(\frac{\hbar\omega}{k_B T}\right) g(\omega)\, d\omega\right]. \tag{1}$$

It is worth noting the temperature-dependent term of Eq. (1) is the same for any configuration. Therefore, in this paper, results for the temperature independent term

$$\bar{S}_{\mathrm{vib}} = -k_B \int \ln(\omega) g(\omega)\, d\omega \tag{2}$$

are presented (with $\omega$ evaluated in units of Hz).

The calculation of the phonon DOS requires a computation of the force-constant tensor $\mathbf{\Phi}(i,j)$, which relates the displacement $u(j)$ of atom $j$ from its equilibrium position to the forces $f(i)$ acting on atom $i$ as follows:

$$f(i) = -\mathbf{\Phi}(i,j)u(j). \tag{3}$$

In order to compute vibrational thermodynamic properties, we employ a first-principles supercell method as a framework for directly calculating values of the interatomic force constants in this work. The basic idea is to perturb atom $j$ away from its equilibrium position by an amount $u(j)$, calculate the force $f(i)$ acting on atom $i$, and then solve a set of linear equations $f(i)=-\mathbf{\Phi}(i,j)u(j)$ to yield the force constant tensor $\mathbf{\Phi}(i,j)$. Normally, the force constants considered have a larger range than the extent of a crystal's primitive unit cell and a supercell composed of several primitive cells must be considered in order to derive the force constants. The method used to construct the supercells and to determine the symmetry-distinct displacements necessary to derive the force constants are as described in Ref. 12, as implemented in the Alloy Theoretic Automated Toolkit (ATAT).[33]

The calculations in this work were carried out using the first-principles program VASP (Vienna *ab initio* simulation package).[34,35] The calculations employed ultrasoft pseudopotentials (treating semicore *p* states as core electrons), and the generalized gradient approximation (GGA) of Perdew and Wang.[36] Electronic wave functions were expanded in plane waves with a kinetic energy cutoff of 281 eV, which is at

least 1.5 times the VASP-default cutoff value for Al, Ti, Zr, and Hf. The Brillouin zone is sampled employing Monkhorst-Pack[37] $k$-point meshes with roughly constant mesh densities for all the fcc-based compounds corresponding to a $20\times20\times20$ grid for the fcc unit cell. The electronic energy levels were broadened using the Methfessel-Paxton scheme[38] with a smearing of 0.1 eV. Convergence tests were conducted for simple structures including fcc Al, *TM* (*TM* =Ti, Zr, and Hf) and the $L1_2$ structure of $Al_3Ti$. The results indicated that with the chosen plane-wave cutoff and $k$-point density the calculated energies are converged to within 0.5 meV/atom.

A 32-atom supercell is used to calculate the vibrational entropy of ordered structures with the first-principles supercell method. The displacement from the equilibrium position for an atom is chosen to have a magnitude of 0.1 Å. For fcc Al, the above settings in the VASP calculations ensure that the calculated stretching and bending force constants (the ratio of the force over the perturbed displacement) were converged to within 0.06 meV/Å$^2$ and 0.01 meV/Å$^2$, respectively (the magnitudes of the respective force constants are 1.27 and −0.0868 eV/Å$^2$). The magnitude of $S_{\mathrm{vib}}$ is found to be highly insensitive to such numerical errors; for fcc Al, this precision in the calculated force constants leads to values of $S_{\mathrm{vib}}$ converged to within $0.0001k_B$/atom. The magnitude of the atomic displacements (0.1 Å) used in the calculation of the force constants was found to lead to an accuracy of about $\pm0.003k_B$/atoms for $S_{\mathrm{vib}}$ (also in fcc Al). The convergence of the calculations with respect to the size of the supercell employed in the force-constant calculations was checked in detail for $Al_3Ti$, and it was found to yield entropies converged to within $0.006k_B$/atom.

In the transferable force constant approach,[12,29–31] three assumptions are made to obtain the desired transferable properties. Only the nearest neighbor interactions are considered (because the longer ranged force constants do not exhibit good transferability). The bending stiffnesses $b$ are averaged over various spatial directions (i.e., to obtain effective isotropic bending stiffnesses), and off-diagonal terms in the bond stiffness tensor $\mathbf{\Phi}$ are constrained to be zero. Hence, the resulting bond stiffness tensor has only two independent terms, namely the stretching stiffness $s$ and the isotropic bending stiffness $b$:

$$\Phi(i,j)=\begin{pmatrix} b & 0 & 0 \\ 0 & b & 0 \\ 0 & 0 & s \end{pmatrix}. \tag{4}$$

Here the coordinate system is transformed so that the $z$ axis is along the direction connecting atom $i$ and $j$. This symmetrization ensures that the force constants never have a symmetry that is lower than the environment into which they are transferred. (It should be noted that it is not possible to retain only $s$, because exclusion of $b$ leads to an error in $S_{\mathrm{vib}}$ on the order of 0.2 $k_B$/atom.[31]) The dependencies of $s$ and $b$ on the bond length $l$ and *TM* concentration are transferable between different chemical environments.

The force constants generated via the TFC method satisfy two important invariance properties that will be shared by the extension we propose. First, the TFC tensors are invariant under the symmetry operations of the crystal's space group and, second, the energy change associated with an infinitesimal translation is zero. These properties are ensured as follows.

Similar chemical bonds in different environments may face different symmetry-induced constraints on their associated spring tensors.[26] The way the TFC method ensures that the transferred force constant tensors always have a symmetry that is compatible with their environment is by using spring tensors that are compatible with the highest possible symmetry, thus implying that they are also compatible with any other environments of a lower symmetry. The highest possible symmetry a chemical bond can have is a cylindrical symmetry, under which only two independent terms remain in the spring tensor: the stretching and bending terms. These are precisely the terms that are assumed to be transferable in the TFC method.

In a Born–von Karman model, the potential energy is invariant under an infinitesimal translation whenever an atom's "self" force constant is equal to minus the sum of all pairwise force constants associated with that atom. In the TFC method, the "self" force constants are not transferred, but are instead explicitly calculated from the transferred pairwise force constants through this sum rule. Translational invariance therefore holds by construction in the TFC method.

The TFC method does not necessarily ensure rotation invariance of the total energy.[54] While imposing rotational invariance will slightly alter the frequencies of all vibrational modes, the only unphysical artifact potentially introduced by not imposing this constrain is to assign a nonzero stiffness to the three rigid rotational modes. In the thermodynamic limit ($N\rightarrow\infty$, where $N$ is the number of atoms), these few degrees of freedom have a negligible impact on any thermodynamic property of the system. Moreover, these rotational degrees of freedom (unlike the translational degrees of freedom) are not sampled during a conventional integration over the Brillouin zone, since pure rotations cannot be expressed as linear combinations of Bloch states. Hence, rotational modes do not even pose practical numerical problems. In any case, Ref. 54 does suggest an avenue to solve this rotational invariance problem, which can be applied to our generalized TFC method, if desired.

In this work, we choose analytic expressions[39] to represent the bond stiffnesses $s$ and $b$ as functions of the bond length $l$ and *TM* concentration $c$, which are derived from a Morse-type potential $\phi(l)$:

$$s=\frac{d^2\phi(l)}{dl^2},$$

$$b=\frac{1}{l}\frac{d\phi(l)}{dl},$$

$$\phi(l)=\frac{D}{2(m-1)l}\{\exp[-m\alpha(l-l_0)]-m\exp[-\alpha(l-l_0)]\}, \tag{5}$$

where $D$, $m$, $\alpha$, and $l_0$ are fitting parameters. Morse functions have been used previously in the modeling of phonon spectra

of bcc Fe and Pd-10%Fe alloys.[39,40] We assume $D$ and $\alpha$ depend on *TM* concentration $c$ explicitly in a polynomial form. The parameter $D$ is represented by a third-order polynomial in $c$, while it was found to be sufficient to assume a linear concentration dependence for $\alpha$. We thus use the following forms in fitting the concentration dependencies of the Morse parameters $D=D_0+D_1c+D_2c^2+D_3c^3$ and $\alpha=\alpha_0+\alpha_1c$.

While simple polynomials have been used to represent the dependence of force constant on bond length in previous applications of the TFC method, we found the use of a Morse potential led to significant improvements in the predictive power of the TFC method for the fcc-based Al-*TM* structures considered in this work. The Morse potential offers the advantage of having, by construction, a physically reasonable shape, unlike a general polynomial which can lead to unphysical predictions outside the range of bond length values for which they are fit. It should be noted that in applying the Morse-potential parametrization to fit the bond-length dependence of the force constants for Al-*TM* compounds, it was necessary to conduct separate fits for $b$ and $s$, i.e., a good fit for bending and stretching force constants could not be obtained with the same set of parameters in Eq. (5). Qualitatively, this result is not surprising since the bonding in Al-*TM* systems is not expected to be well described by pair potentials, and the fact that different parametrizations for $s$ and $b$ are required likely reflects the significance of the many-body and/or angular contributions to the interatomic potentials in these systems.

The TFC algorithms described above have been implemented in the Alloy Theoretic Automated Toolkit (ATAT).[33,41] This code includes utilities for performing the supercell calculations to derive force constants, for diagonalizing the dynamical matrices to obtain phonon densities of states (DOS), for integrating the phonon DOS to compute vibrational free energies and entropies, and for fitting and utilizing the transferable force constant approach to simplify the calculations of vibrational thermodynamic properties.

Finally, it should be noted that all of the results presented in the next section have been derived within the harmonic approximation, employing the bond lengths corresponding to relaxed structures at zero temperature. The magnitude of anharmonic contributions, derived within the quasiharmonic approximation, are discussed in Sec. IV, where a comparison of calculated formation entropies to available experimental data for the Al-Ti system is presented.

## III. RESULTS

### A. Direct vibrational-entropy calculations

Vibrational entropies have been calculated for fcc Al, fcc Ti, and $L1_2$ $Al_3Ti$ using the first-principles supercell method described in the previous section. To provide reference values for assessing the accuracy of the TFC approximations listed above, calculations of the vibrational entropy for these three structures were computed as a function of the range of the force constants in a 64-atom supercell. As reported in Table I, the results computed with first nearest neighbor (1NN) force constants versus those derived with first-fifth nearest neighbor force constants (5NN) differ by less than $0.05k_B$/atom for the high-temperature limits of the vibrational entropy $S_{\mathrm{vib}}$ and vibrational entropy of mixing $\Delta S_{\mathrm{vib}}$. The latter quantity ($\Delta S_{\mathrm{vib}}$) is defined as the difference in vibrational entropy between an alloy and a concentration weighted average of $S_{\mathrm{vib}}$ for the constituent pure elements in the fcc crystal structure: $\Delta S_{\mathrm{vib}}(\mathrm{Al}_x TM_{(1-x)}) = S_{\mathrm{vib}}(\mathrm{Al}_x TM_{(1-x)}) - xS_{\mathrm{vib}}(\mathrm{Al},\mathrm{fcc}) - (1-x)S_{\mathrm{vib}}(TM,\mathrm{fcc})$. The error in the calculated vibrational entropies associated with truncating the range of the force constants to the first nearest neighbor (1NN) shell is estimated to be less than 5% of the magnitude. This relatively small error justifies the truncation of the force constants at 1NN in the application of the TFC method below.

The vibrational entropies of mixing for 23 selected ordered structures, calculated with the first-principles supercell method employing a 1NN truncation of the forces constants, are presented in Table II (third column). For completeness, the values of the mixing energy $\Delta E$ calculated with the same electronic-structure method are also provided (second column in Table II). By analogy with the mixing entropy, $\Delta E$ represents the energy difference between an alloy and concentration weighted average of the energy of elemental fcc Al and *TM*: $\Delta E(\mathrm{Al}_x TM_{(1-x)}) = E(\mathrm{Al}_x TM_{(1-x)}) - xE(\mathrm{Al},\mathrm{fcc}) - (1-x)E(TM,\mathrm{fcc})$. The negative values of $\Delta S$ and $\Delta E$ for all of the ordered structures considered are consistent with the strong ordering tendencies displayed by these Al-*TM* (*TM* =Ti, Zr, and Hf) systems. Specifically, the formation of strong Al-*TM* bonds in the compounds leads to a lower energy and vibrational entropy relative to the constituent pure elements. We note that the presently calculated values of the vibrational entropy of mixing for $Al_3Zr$ compounds, $\Delta S_{\mathrm{vib}}(L1_2\text{-}Al_3Zr) = -0.820k_B$/atom and $\Delta S_{\mathrm{vib}}(D0_{23}\text{-}Al_3Zr) = -0.896k_B$/atom, agree well with the results $\Delta S_{\mathrm{vib}}(L1_2\text{-}Al_3Zr) = \Delta S_{\mathrm{vib}}(D0_{23}\text{-}Al_3Zr) = -0.85k_B$/atom obtained by Clouet *et al.*[42] using a full-potential implementation of the linear response (LR) method, and the local-density approximation (LDA).

### B. Parametrization of the transferable force constants

Calculated 1NN force constant matrices for 17 fcc-based structures in the three Al-*TM* systems (labeled with "+" symbols in Table II) are transformed to the stretching-isotropic bending form given in Eq. (4). The dependencies of the $s$ and $b$ force constants on bond length $l$ and the *TM* concentration are plotted in Figs. 1–3, in which the symbols represent different *TM* concentrations, as described in the insets.

In Figs. 1–3, the stretching force constants $s$ decrease monotonically with increasing bond length. The bending terms, by contrast, are relatively insensitive to changes in bond length. The dependence of $s$ and $b$ on *TM* concentration can be clearly observed for Al–Al and *TM*–*TM* bonds. It is, therefore, not surprising that relying on the bond length versus bond stiffness relation alone, as a basis for transferring force constants between structures, is not found to be an accurate approach in these systems. The curves in Figs. 1–3 are the fitted relations derived from the formulas given in Eq.

TABLE I. The temperature independent term of the vibrational entropy $\bar{S}_{\mathrm{vib}}$ and vibrational entropies of mixing $\Delta S_{\mathrm{vib}}$ (in units of $k_B$/atom) calculated by the first-principles supercell method. Results are calculated with force constants in the full matrix formula (calc, fc) truncated at first nearest neighbor (1NN) to fifth nearest neighbor (5NN) distances. The differences between results obtained with 1NN versus 5NN truncation of the force constants are also indicated.

| | | Range of force constants | | | | | |
|---|---|---|---|---|---|---|---|
| | Structures | 1NN | 2NN | 3NN | 4NN | 5NN | Errors $[S_{\mathrm{vib}}^{\mathrm{calc,fc}}(1\mathrm{NN}) - S_{\mathrm{vib}}^{\mathrm{calc,fc}}(5\mathrm{NN})]$ |
| $S_{\mathrm{vib}}^{\mathrm{calc,fc}}$ | Al fcc | −88.114 | −88.133 | −88.130 | −88.127 | −88.130 | 0.016 |
| | Ti fcc | −87.342 | −87.275 | −87.310 | −87.285 | −87.288 | −0.054 |
| | $Al_3Ti(L1_2)$ | −88.750 | −88.772 | −88.786 | −88.783 | −88.784 | 0.034 |
| $\Delta S_{\mathrm{vib}}$ | $Al_3Ti(L1_2)$ | −0.829 | −0.854 | −0.861 | −0.867 | −0.865 | 0.036 |

TABLE II. Vibrational entropies of mixing (in units of $k_B$/atom) calculated by both the first-principles supercell method and the transferable force constant (TFC) approach. The energy of mixing (in units of meV/atom) is presented in second column. The symbol $\Delta S_{\mathrm{vib}}^{\mathrm{calc,fc}}$ represents the results obtained by the first-principles supercell method with force-constants truncated at first nearest neighbor (1NN). The symbol $\Delta S_{\mathrm{vib}}^{\mathrm{calc,sb}}$ represents results of calculations with force constant tensors represented in the stretching and isotropic bending approximation represented by Eq. (4). Finally, the symbol $\Delta S_{\mathrm{vib}}^{\mathrm{fit,sb}}$ represents results derived by the TFC method employing the stretching and isotropic bending approximations, with force constants represented from fits of the Morse-potential parameters defined in Eq. (5). The structures labeled by (+) are used in fitting the Morse potential parameters. In all, results are presented for 23 ordered structures identified by their stoichiometry. Detailed descriptions of these 23 ordered structures are presented in the Appendix.

| Structure | $\Delta E$ | $\Delta S_{\mathrm{vib}}^{\mathrm{calc,fc}}$ | $\Delta S_{\mathrm{vib}}^{\mathrm{calc,sb}}$ | $\Delta S_{\mathrm{vib}}^{\mathrm{fit,sb}}$ | Fitting | $(\Delta S_{\mathrm{vib}}^{\mathrm{calc,sb}} - \Delta S_{\mathrm{vib}}^{\mathrm{calc,fc}})$ | $(\Delta S_{\mathrm{vib}}^{\mathrm{fit,sb}} - \Delta S_{\mathrm{vib}}^{\mathrm{calc,sb}})$ | $(\Delta S_{\mathrm{vib}}^{\mathrm{fit,sb}} - \Delta S_{\mathrm{vib}}^{\mathrm{calc,fc}})$ |
|---|---|---|---|---|---|---|---|---|
| $Al_3Ti$ $(L1_2)$ | −395.09 | −0.835 | −0.841 | −0.922 | + | −0.006 | −0.080 | −0.087 |
| $Al_3Ti$ $(D0_{22})$ | −421.10 | −0.873 | −0.892 | −0.842 | | −0.019 | 0.050 | 0.031 |
| $Al_3Ti$ $(D0_{23})$ | −428.09 | −0.922 | −0.933 | −0.894 | | −0.011 | 0.039 | 0.028 |
| $Al_2Ti$ $(Cmmm,65)$ | −453.79 | −0.949 | −0.965 | −0.913 | + | −0.016 | 0.052 | 0.036 |
| $Al_5Ti_3$ $(Cmmm,65)$ | −416.97 | −0.864 | −0.875 | −0.896 | + | −0.011 | −0.021 | −0.032 |
| $AlTi$ $(L1_0)$ | −438.18 | −0.862 | −0.870 | −0.922 | + | −0.008 | −0.051 | −0.060 |
| $Al_3Ti_5$ $(Cmmm,65)$ | −348.16 | −0.749 | −0.766 | −0.825 | + | −0.016 | −0.059 | −0.075 |
| $AlTi_3$ $(L1_2)$ | −307.26 | −0.685 | −0.702 | −0.683 | + | −0.017 | 0.019 | 0.002 |
| $Al_3Zr$ $(L1_2)$ | −490.35 | −0.820 | −0.838 | −0.844 | + | −0.018 | −0.006 | −0.024 |
| $Al_3Zr$ $(D0_{22})$ | −492.35 | −0.789 | −0.839 | −0.707 | | −0.050 | 0.132 | 0.083 |
| $Al_3Zr$ $(D0_{23})$ | −518.35 | −0.896 | −0.924 | −0.786 | | −0.028 | 0.138 | 0.110 |
| $Al_2Zr$ $(Cmmm,65)$ | −547.52 | −0.899 | −0.923 | −0.912 | + | −0.024 | 0.010 | −0.013 |
| $Al_5Zr_3$ $(Pmmm,47)$ | −513.34 | −0.861 | −0.886 | −0.845 | + | −0.025 | 0.041 | 0.016 |
| $AlZr$ $(L1_0)$ | −483.70 | −0.772 | −0.777 | −0.695 | + | −0.005 | 0.082 | 0.077 |
| $Al_3Zr_5$ $(I4/mmm,139)$ | −417.84 | −0.731 | −0.742 | −0.711 | + | −0.011 | 0.030 | 0.019 |
| $AlZr_3$ $(L1_2)$ | −346.04 | −0.687 | −0.703 | −0.514 | + | −0.016 | 0.189 | 0.173 |
| $Al_3Hf$ $(L1_2)$ | −399.93 | −0.738 | −0.747 | −0.817 | + | −0.009 | −0.070 | −0.079 |
| $Al_3Hf$ $(D0_{22})$ | −417.93 | −0.759 | −0.803 | −0.733 | | −0.043 | 0.070 | 0.026 |
| $Al_3Hf$ $(D0_{23})$ | −428.93 | −0.828 | −0.850 | −0.789 | | −0.023 | 0.062 | 0.039 |
| $Al_5Hf_3$ $(P1,1)$ | −427.78 | −0.776 | −0.793 | −0.810 | + | −0.017 | −0.017 | −0.034 |
| $AlHf$ $(L1_0)$ | −400.73 | −0.679 | −0.691 | −0.595 | + | −0.012 | 0.096 | 0.083 |
| $Al_3Hf_5$ $(P4/mmm,123)$ | −203.48 | −0.661 | −0.672 | −0.646 | + | −0.011 | 0.026 | 0.015 |
| $AlHf_3$ $(L1_2)$ | −303.58 | −0.679 | −0.685 | −0.628 | + | −0.006 | 0.057 | 0.050 |

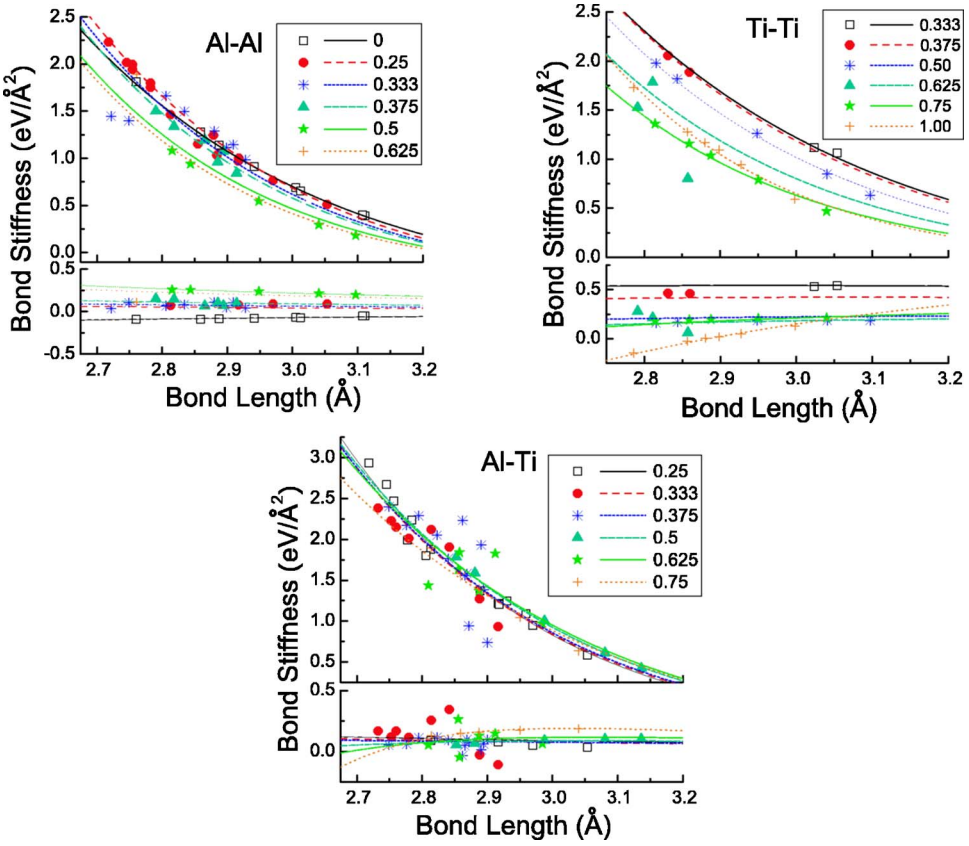


FIG. 1. (Color online) Nearest-neighbor stretching and bending force constants in Al-Ti alloys versus bond length and Ti concentration. The upper figures are for the stretching force constants and the figures below are for the bending force constants. The symbols represent results calculated from the first-principles supercell method for different Ti concentrations, as described in the inset. The curves are fitted functions with the form given in Eq. (5) for different Ti concentrations depicted in the inset.

(5). The fitting parameters and the root-mean-square fitting errors are listed in Table III. Although the bending force constants could have been represented by a much simpler linear length dependence, we also used a separate Morse functional form, for simplicity in the implementation of the method. However, given the featureless nature of the behavior of the bending force constants, the resulting parameters do not necessarily have physically meaningful values, they are merely constants that produced reasonable fits to the average bending stiffnesses.

Surprisingly, there is an apparent discrepancy between the parameter values obtained for Al–Al bonds in the limit of pure Al in the different alloy systems considered here. However, this is mostly an artifact of the functional form chosen; very different parameter values in the modified Morse potential can yield very similar shapes for the stiffness-length relationship. In fact, as seen in the upper left graphs in Figs. 1–3, if one superimposes the predicted stiffness-length relationships for Al–Al bonds in pure Al for all three systems, they would overlap nearly perfectly.

### C. Accuracy of entropies derived from transferable force constants

With the fitted relations shown in Figs. 1–3 it is possible to estimate the magnitudes of the stretching and bending force constants for any structure from a knowledge of its equilibrium bond lengths and concentration. To assess the accuracy of the entropies derived from these fitted relations, we can compare the TFC predictions for $\Delta S_{\mathrm{vib}}$ with those derived directly from supercell calculations performed within the isotropic bending 1NN approximation.

Consider first a comparison between the predictions of the TFC method and the directly calculated results for the structures listed in Table II which were used in the fitting (indicated with + symbols in column four). This comparison provides an indication of the quality of the fit resulting from the parametrization of the force constants. In Fig. 4 the TFC and directly calculated values of the mixing entropies are plotted as filled and open symbols, respectively. The values are also compared in Tables I and II. Specifically, the errors are summarized in the order of the three assumptions we have adopted. (1) As illustrated by the results for $Al_3Ti$ $L1_2$ in Table I, the 1NN assumption introduces an error of about $0.036k_B$/atom (4% of the magnitude of $\Delta S_{\mathrm{vib}}$). (2) In Table II, $\Delta S_{\mathrm{vib}}$ values calculated with the full force constant matrix and the $\Delta S_{\mathrm{vib}}$ calculated with the stretching + isotropic-bending force-constant model [Eq. (4)], agree within $0.025k_B$/atom (3% of the magnitude of the $\Delta S_{\mathrm{vib}}$). (3) The $\Delta S_{\mathrm{vib}}$ difference between the results calculated by the TFC method using the fitted parameters and by the stretching + isotropic-bending model are less than $0.1k_B$ the structures (except $AlZr_3$ $L1_2$ where the difference is about $0.2k_B$/atom). Because error cancellation occurs between the second (stretching-bending model) and the third (stretching-bending force constant fitting) assumptions, the $\Delta S_{\mathrm{vib}}$ difference between the TFC results and the 1NN full-force-constant calculations are less than $0.18k_B$/atom. Overall, the error is less than $0.176k_B$/atom, i.e., roughly 20% of the well converged mixing vibrational entropy calculated by first-principles.

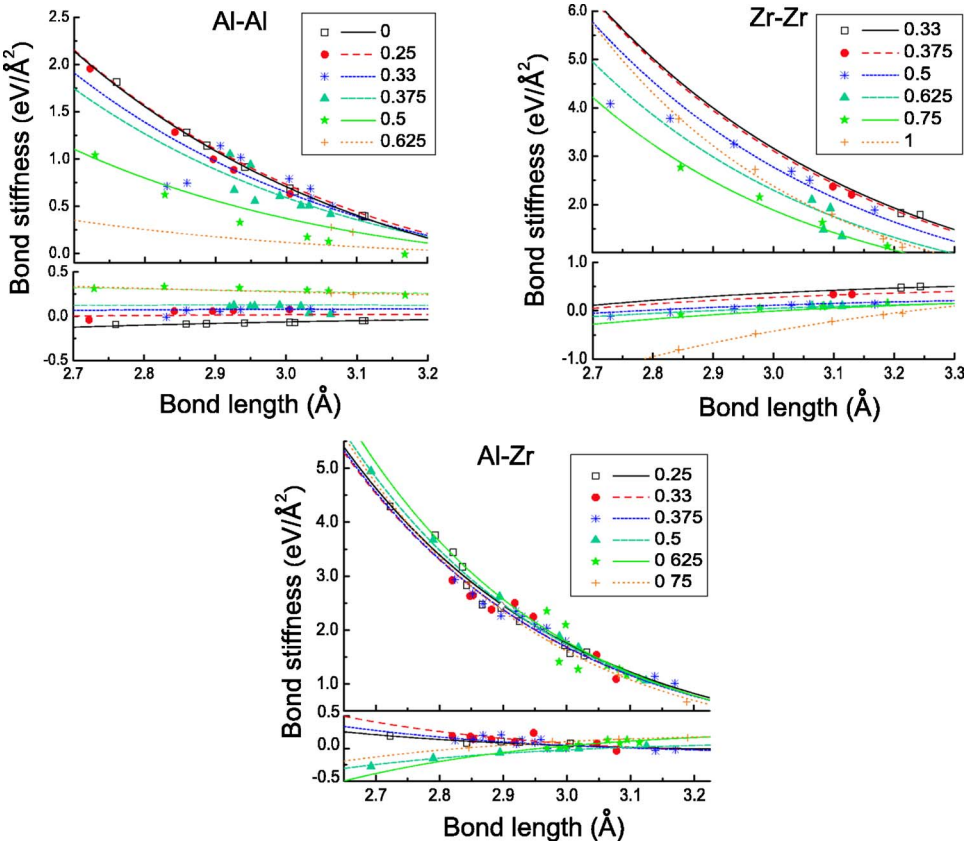


FIG. 2. (Color online) Nearest-neighbor stretching and bending force constants in Al-Zr alloys versus bond length and Zr concentration. The upper figures are for the stretching force constants and the figures below are for the bending force constants. The symbols represent results calculated from the first-principles supercell method for different Zr concentrations, as described in the inset. The curves are fitted functions with the form given in Eq. (5) for different Zr concentrations depicted in the inset.

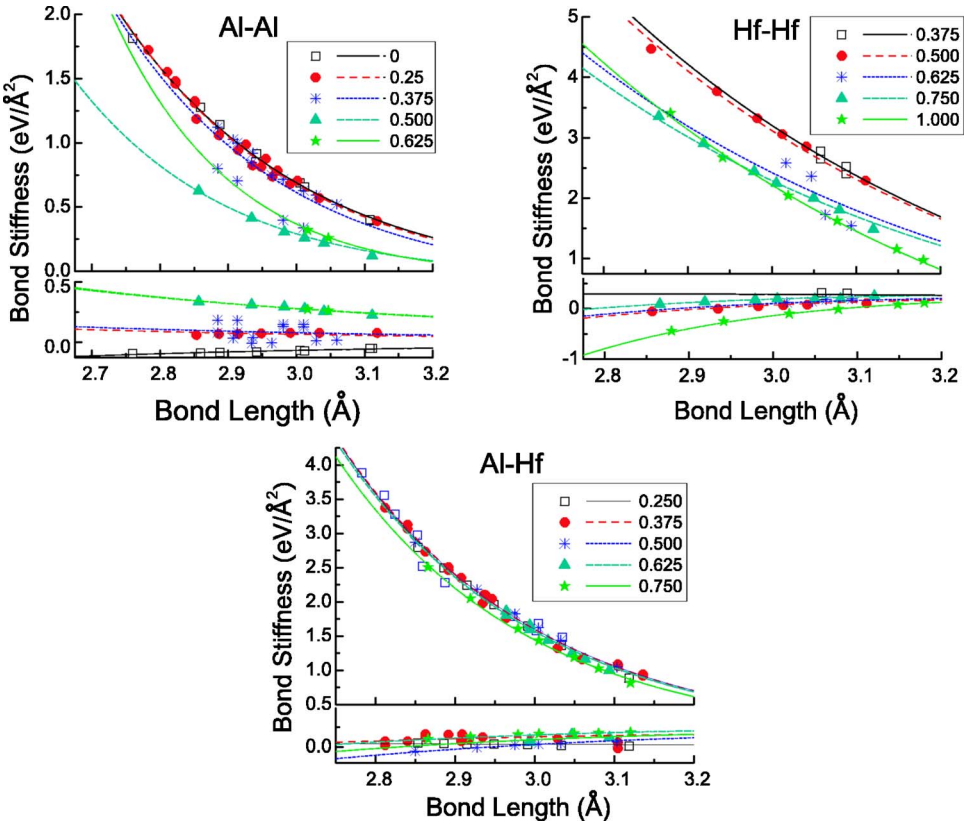


FIG. 3. (Color online) Nearest-neighbor stretching and bending force constants in Al-Hf alloys versus bond length and Hf concentration. The upper figures are for the stretching force constants and the figures below are for the bending force constants. The symbols represent results calculated from the first-principles supercell method for different Hf concentrations, as described in the inset. The curves are fitted functions with the form given in Eq. (5) for different Hf concentrations depicted in the inset.

TABLE III. Fitted parameters in Eq. (5) for the transferable force constants in fcc-based Al-*TM* (*TM* =Ti, Zr, and Hf) alloys.

| | | Al-Al | | Al-Ti | | Ti-Ti | |
|---|---|---|---|---|---|---|---|
| | | *s* | *b* | *s* | *b* | *s* | *b* |
| $D_0$ | (eV Å) | 8.03 | −30.81 | 4.923 | 5.976 | 6.605 | 1179 |
| $D_1$ | (eV Å) | −13.16 | 232.9 | −11.28 | −1.037 | −18.82 | −3953 |
| $D_2$ | (eV Å) | −3.86 | −619.2 | 36.66 | −22.83 | 18.63 | 4191 |
| $D_3$ | (eV Å) | 14.13 | 506.7 | −10.31 | 26.45 | −6.200 | −752.9 |
| $\alpha_0$ | ($Å^{-1}$) | 0.999 | 0.001655 | 1.752 | −0.7769 | 0.7809 | 0.1314 |
| $\alpha_1$ | ($Å^{-1}$) | 1.066 | 0.001791 | −1.091 | 2.67 | 1.802 | 0.006798 |
| $m$ | | 1.13 | 0.9574 | 0.9921 | 3.782 | 1.001 | 0.4308 |
| $l_0$ | (Å) | 2.863 | 588 | 2.887 | 2.786 | 3.203 | 11.34 |
| r.m.s. | ($eV/Å^2$) | 0.089 | 0.03098 | 0.2492 | 0.07582 | 0.07929 | 0.066 |
| | | Al-Al | | Al-Zr | | Zr-Zr | |
| | | *s* | *b* | *s* | *b* | *s* | *b* |
| $D_0$ | (eV Å) | 22.75 | 25.94 | 5.032 | 120.3 | 26.04 | 3431 |
| $D_1$ | (eV Å) | −23.21 | −456.6 | −15.03 | −944.7 | −64.4 | −10470 |
| $D_2$ | (eV Å) | −47.17 | 2290 | 27.04 | 2163 | 53.13 | 9883 |
| $D_3$ | (eV Å) | 47.63 | −2387 | −17.65 | −1445 | −13.22 | −1104 |
| $\alpha_0$ | ($Å^{-1}$) | 0.7425 | 0.2056 | 1.557 | 1.902 | 0.5795 | 0.1339 |
| $\alpha_1$ | ($Å^{-1}$) | 0.4344 | −0.05066 | 0.6819 | −1.031 | 0.9173 | 0.002032 |
| $m$ | | 0.9973 | 0.2955 | 0.7014 | 0.216 | 1.014 | 0.09145 |
| $l_0$ | (Å) | 2.8695 | 9.615 | 3.209 | 3.535 | 3.471 | 19.97 |
| r.m.s. | ($eV/Å^2$) | 0.1031 | 0.03102 | 0.1817 | 0.04184 | 0.0976 | 0.05971 |
| | | Al-Al | | Al-Hf | | Hf-Hf | |
| | | *s* | *b* | *s* | *b* | *s* | *b* |
| $D_0$ | (eV Å) | 11.79 | −5.037 | 0.5543 | 426.9 | 30.45 | 430.7 |
| $D_1$ | (eV Å) | −12.75 | 84.47 | −0.2675 | −3271 | −68.01 | −2068 |
| $D_2$ | (eV Å) | −20.1 | −292.4 | 0.7896 | 7352 | 51.71 | 3147 |
| $D_3$ | (eV Å) | 22.2 | 409.1 | −0.8153 | −4896 | −11.88 | −1477 |
| $\alpha_0$ | ($Å^{-1}$) | 0.3211 | −0.2819 | 3.592 | 0.3502 | 0.7014 | 1.224 |
| $\alpha_1$ | ($Å^{-1}$) | 0.2038 | 0.5805 | 0.08942 | −0.1008 | 1.020 | 1.461 |
| $m$ | | 5.857 | 0.02785 | 0.05616 | 0.8691 | 1.000 | 0.003172 |
| $l_0$ | (Å) | 2.984 | 39.4 | 3.827 | 4.949 | 3.190 | 4.408 |
| r.m.s. | ($eV/Å^2$) | 0.08496 | 0.018 | 0.07576 | 0.046 | 0.1853 | 0.05 |

Next we consider the predictions of the TFC method for structures not included in the fitting of the force-constant parametrizations. Specifically, we focus on $D0_{22}$ and $D0_{23}$ $Al_3TM$ (*TM*=Ti, Zr, and Hf) structures which were not included in the fit of the transferable force-constant relations. The results for these structures can be taken as tests of the predictive power of the TFC method. In Table II, the second approximation has a slightly larger error, $0.05k_B$/atom and the third additionally introduces an error as large as $0.14k_B$/atom. The same error cancellation as noted for $L1_2$ occurs between the second and third approximations, and the overall errors for $D0_{22}$ and $D0_{23}$ structures are less than $0.11k_B$/atom or about 10%. In addition to the $0.036k_B$/atom error resulting from 1NN force constant assumption, the total error is about $0.146k_B$/atom, which is comparable to the errors in reproducing the vibrational entropy of the structures involved in the fitting of the TFC relations. Overall the level of error estimated in the values of $\Delta S_{\text{vib}}$ obtained with the 1NN TFC approach is within approximately 20% of the overall magnitude of the most well converged results.

### D. Vibrational entropy cluster expansions

The transferable force constant approach represents an efficient computational framework for calculating the vibrational entropy and is a convenient tool for the construction of vibrational-entropy cluster expansions. In this approach, the parameters describing the dependencies of *s* and *b* upon bond length and concentration are fit to a small number of first-principles supercell calculations. For a new structure,

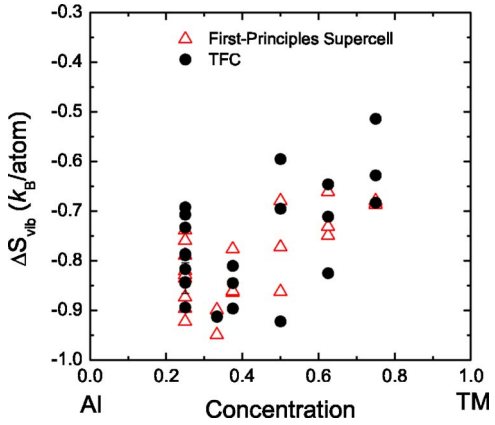


FIG. 4. (Color online) Comparison of $\Delta S_{vib}$ calculated by the first-principles supercell method (open triangles) and the transferable force constant approach (solid circles) for the ordered structures listed in Table II.

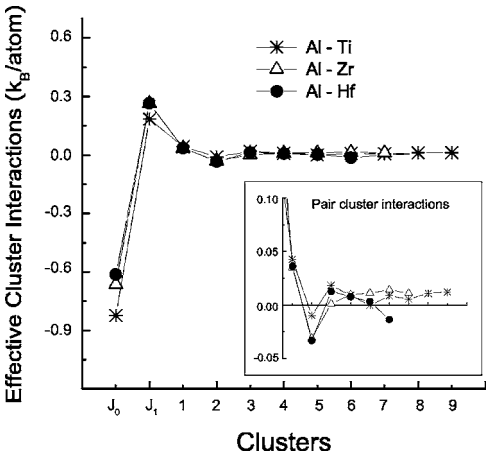


FIG. 5. The cluster interaction parameters (effecitve cluster interactions) used in our vibrational entropy cluster expansions. Here $J_0$ and $J_1$ represent empty and point clusters, respectively. "1" represents first nearest neighbor, "2" represents second nearest neighbor, and so on. The inset figure shows the interactions just for pair clusters.

the relaxed bond lengths and *TM* concentration are sufficient information to determine estimates of the force constants for the calculation of the phonon DOS and the vibrational entropy. The TFC method makes use of the feature that the relaxed geometry of the structure is a by-product of the first-principles energy calculations, which are needed in the energy cluster expansion used in phase diagram calculations, whether or not vibrational effects are considered. Thus, the efficiency of the TFC method is associated with its ability to estimate the force constants for new structures requiring only total-energy calculations using a primitive unit cell, instead of large supercells to determine the force constants. In this section we present the application of this method in the construction of $\Delta S_{vib}$ cluster expansions for fcc-based structures in each of the three Al-*TM* (*TM*=Ti, Zr, and Hf) systems considered.

Aided by the TFC method, the vibrational entropies of approximately 30 ordered fcc-based superstructures were calculated for each of the three Al-*TM* (*TM*=Ti, Zr, and Hf) systems, and used in constructing the cluster expansions for the mixing vibrational entropy $\Delta S_{vib}$. Figure 6 plots the results, comparing the TFC-calculated and cluster-expansion (CE) fitted values for ordered alloy configurations (open and filled symbols, respectively) as well as the CE predictions for random fcc-based solid solutions (solid line). The details related to the cluster-expansion fits are summarized in Table IV and Fig. 5. It is noted that to obtain cluster expansions with cross-validation (CV) scores within about 10% of the magnitude of the mixing entropies, fairly long-ranged interactions are required. For the Al-Ti system, in particular, pair interactions up to ninth neighbor were required, in addition to a number of fairly long-ranged triplet cluster interactions. Figure 5 plots the interaction parameters [effective cluster interactions (ECIs)] for empty, point and pair clusters used in our vibrational entropy cluster expansions. The contributions from triplet and quadruplet clusters are much smaller. Their interaction parameters are one to two orders of magnitude less than the first nearest neighbor pair interactions. Further details related to the cluster-expansion fits can be found in Ref. 43.

TABLE IV. Details related to the cluster-expansion fits for the mixing vibrational entropy ($\Delta S_{vib}$). *N* is the number of structures used in the cluster-expansion fitting.

| | | Number of clusters | | | | |
|---|---|---|---|---|---|---|
| | *N* | Pair | Triplet | Quadruplet | Total | CV score ($k_B$/atom) |
| Al-Ti | 43 | 9 | 5 | 1 | 17 | 0.0759 |
| Al-Zr | 36 | 7 | 3 | 1 | 13 | 0.0634 |
| Al-Hf | 28 | 6 | 3 | 3 | 14 | 0.0882 |

## IV. DISCUSSION

In this work significant effort was devoted to developing and testing the accuracy of a TFC method in its application to the calculation of vibrational entropies in Al-*TM* (*TM*=Ti, Zr, and Hf) systems. It is interesting to compare the results related to these tests with comparable analyses performed for late-transition and noble-metal alloys in previous work by Wu *et al.*[31] Compared to the systems considered in the present work, the noble-metal systems considered by Wu *et al.* display much weaker driving forces for alloying, i.e., the mixing energies are much smaller in magnitude. For the present systems the errors associated with the prediction of $S_{vib}$, arising from application of the TFC method (including composition dependence of the force constants) are larger in an absolute sense, i.e., about $0.15k_B$/atom versus $0.06k_B$/atom in the work of Wu *et al.* In light of the larger magnitude of the mixing vibrational entropies in the present work, i.e., about $-0.8k_B$/atom versus $0.1-0.15k_B$/atom for the late-transition and noble-metal systems, the relative error is actually smaller for the fcc-based Al-*TM* alloys.

The transferable force constant approach presented in this paper exhibits two new features which were not observed in

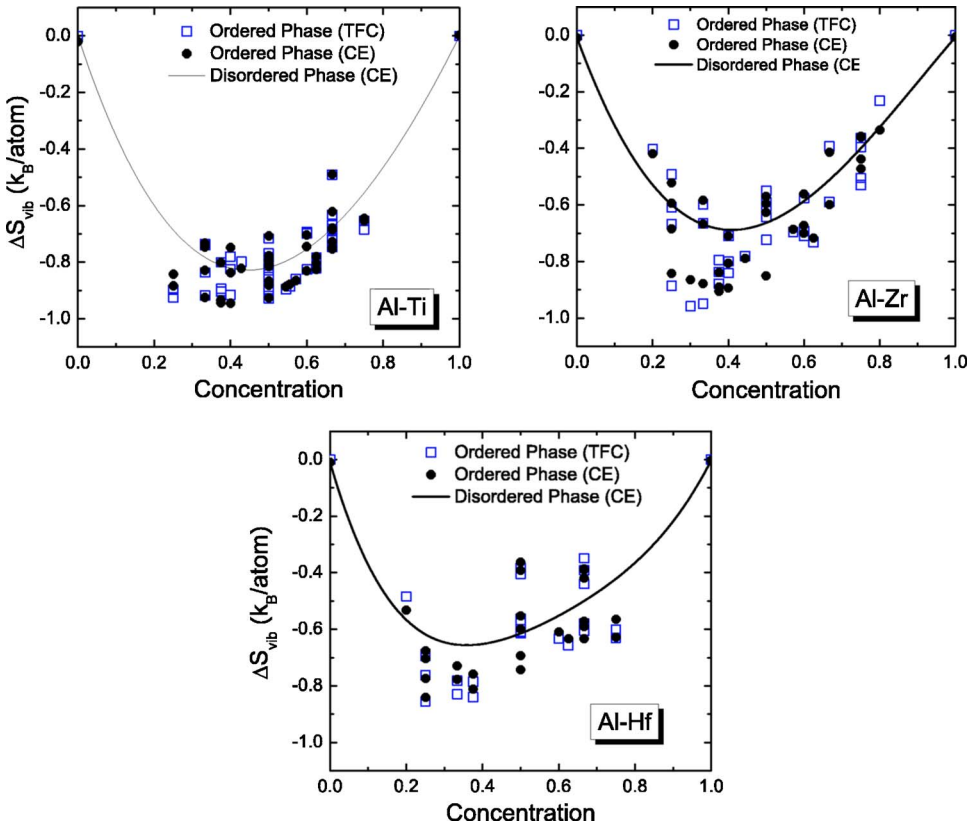


FIG. 6. (Color online) Vibrational entropies of mixing versus *TM* (*TM*=Ti, Zr, and Hf) concentration. The symbols represent the results for selected ordered structures. Open squares are the results calculated by the transferable force constant approach while the solid circles are the values predicted by the cluster expansion (CE). The solid lines are the CE predictions for a random disordered solid solution phase.

previous work by van de Walle *et al.*[12,29,30] and Wu *et al.*[31] In the Al-*TM* (*TM*=Ti, Zr, and Hf) alloys, Al–Al and *TM*–*TM* bond force constants exhibit strong dependencies on the *TM* concentration in addition to the equilibrium bond lengths, as shown in Figs. 1–3. In fact, this concentration dependence explains some of the scatter in the fit of the stiffness versus length relationships found in a previous study of the Al-Ti system.[14] Furthermore, the *TM*-*TM* stretching force constants plotted in Figs. 1–3 show a trend towards increasing stiffness with increasing *TM* concentration; for the Al–Al bonds there is also an overall tendency towards softening of the bonds with increasing *TM* concentration, as seen most clearly in Figs. 2 and 3. In Ref. 31, Wu *et al.* found that in Au-Cu, Au-Pd, and Cu-Pd systems, the force constants of a given bond type (e.g., Au-Au or Pd-Pd) were highly transferable between different chemical systems. This is clearly not the case in the Al-*TM* systems considered here, where the Al–Al bond force constants exhibit clear differences

TABLE V. Calculated and measured thermodynamic properties for Al-Ti intermetallic compounds.

| | $Al_3Ti$ | | | AlTi | | |
|---|---|---|---|---|---|---|
| | $\Delta G$ (eV/atom) $T$=850 K | $\Delta H$ (eV/atom) | $\Delta S$ ($k_B$/atom) $T$=850 K | $\Delta G$ (eV/atom) $T$=973 K | $\Delta H$ (eV/atom) | $\Delta S$ ($k_B$/atom) $T$=973 K |
| Expt. | −0.3199[a] | −0.379±0.011[b] | −1.030[f] | −0.3267 | −0.416±0.010[b] | |
| | | −0.368±0.010[c] | | | −0.377±0.010[c] | |
| | | −0.379±0.013[d] | | | −0.364±0.005[e] | |
| | | −0.406±0.019[e] | | | | |
| VASP-GGA[g] | | −0.409 | | | −0.417 | |
| 3NN Harmonic | −0.342 | | −0.822 | −0.333 | | −0.694 |
| 3NN Quasiharmonic | −0.335 | | −1.020 | −0.324 | | −0.855 |

[a]Reference 52.
[b]Reference 47.
[c]Reference 48.
[d]Reference 49.
[e]Reference 50.
[f]Reference 53, obtained by linear interpolation of results reported at 800 and 900 K.
[g]Reference 32.

amongst the three *TM* (*TM*=Ti, Zr, and Hf) alloy systems.

The concentration dependence of the force constants for the Al-*TM* systems are likely to be the consequence of the electronic charge transfer from Al–Al bonds to *TM*–*TM* and Al–*TM* bonds associated with alloying. The bonding in Al–*TM* structures has been discussed in detail by Zou and Fu[44] (see also a review of the literature on this topic given in Ref. 45). A major feature of the bonding is the strong hybridization between Al *p* and *TM d* electrons. When alloying Al with *TM* (*TM*=Ti, Zr, and Hf) atoms, charge is transferred from the Al–Al to the Al–*TM* bonds. At higher *TM* concentration, *TM*–*TM* bonds play an increasingly important role in the cohesive properties and increasing transfer of charge to these bonds is found. It is reasonable to assume the magnitude of the charge-transfer effect depends on the type of *TM* atom (i.e., electronegativity differences) and it is perhaps not surprising that the Al–Al bond-stretching force constants show a concentration dependence that varies in magnitude between the three Al–*TM* systems.

It is worth noting that local chemical environment also appears to have an effect on the magnitude of the force constants. In Fig. 1, significant scatter in Al–Al and Al–Ti bond stiffnesses for fixed compositions of $c=0.375$ and 0.333 is observed in the Al–Ti system. An analysis of these results shows that the two Al–Al bonds with force constants deviating significantly from the fitted values in Fig. 1 have six Al–Ti bonds in their nearest-neighbor coordination shell, while for the other Al-Al bonds derived from structures with the same compositions, the number of Al–Ti bonds is only four. For the TFC method to take into account these local-environment dependencies, significantly more work would be needed to parametrize the force constants. Fortunately, the scatter in the force constants displayed in Fig. 1 does not appear to introduce very large errors according to the accuracy tests presented in Table II. We note that the TFC method can be viewed as a specific type of interatomic-potential model optimized for the calculation of vibrational thermodynamic calculations. Relative to a more general interatomic potential model, developed to describe energies of arbitrary arrangements of atoms, the fitting procedure for the TFC is considerably simpler and more systematic than for a classical potential model due to the fact that this method aims to predict energies only in the vicinity of the equilibrium geometry for atomic arrangements with a given fixed underlying parent lattice. While the TFC approach thus represents a restricted parametrization, it nevertheless provides important insights into the features of the bonding in the system that must be included in a more detailed interatomic potential model. Specifically, in the present case the concentration dependencies of the bond stiffnesses, presumably arising from charge-transfer effects, would need to be accounted for in a potential model capable of accurately modeling thermodynamic properties in these Al-*TM* systems.

As a final comment concerning the accuracy of the TFC approach, it should be noted that in some cases the method is not able to correctly predict the relative ordering in the magnitude of the vibrational entropies of mixing for ordered alloy compounds at a fixed composition. Specifically, the 1NN full force constant supercell calculations yield $Al_3Ti$ vibrational entropies with values in the following order: $\Delta S_{vib}(L1_2) > \Delta S_{vib}(D0_{22}) > \Delta S_{vib}(D0_{23})$, while the TFC results predict $L1_2$ to have the smallest value. It is to be emphasized, however, that the vibrational entropy differences between these structures is extremely small (less than $0.08k_B$/atom) and within the magnitude of the errors estimated above. Considering the complex nature of the bonding in Al-*TM* systems, it is overall quite encouraging that a simple transferable force constant approach appears to be reasonably successful in computing the vibrational entropy with substantially reduced computational requirements, provided that the simple addition of the concentration dependence to the parametrization of the force constants is accounted for.

In Fig. 6, the mixing vibrational entropy $\Delta S_{vib}$ results are seen to be large and negative over the entire concentration range, for all of the ordered structures, as well as the disordered solid solutions. This result is consistent with the observed strong ordering tendencies displayed by these Al-*TM* (*TM*=Ti, Zr, and Hf) alloys. It is also observed that the vibrational entropies of mixing for disordered phases (solid curves in Fig. 6) show a clear asymmetric behavior, with magnitudes skewed toward Al rich concentrations. Similar trends have been observed[46] for calculated mixing energies of disordered Al-*TM* alloys. We qualitatively attribute these phenomena to the nature of the bonding in Al-*TM* alloys. In the Al rich region, the strong *p*-*d* hybridization results in an increased occupation of bonding states, and thus results in a lower bond energy and a stronger bond stiffness.[32] As a result, the vibrational entropy of mixing is relatively lower (more negative) in Al-rich region.

For the Al-Ti system both calorimetry[47–50] and EMF measurements[51,52] have been performed for the thermodynamic properties of solid-phase alloys.[53] The two experimentally observed fcc-based Al-Ti compounds considered in this work are the $D0_{22}$ $Al_3Ti$ and $L1_0$ AlTi phases. In Table V we compare calculated values of the formation values for the enthalpy ($\Delta H$), entropy ($\Delta S$), and Gibbs free energy ($\Delta G$). In this table, formation quantities are defined as the difference between the thermodynamic property for the compound minus the concentration-weighted average of the corresponding quantities for fcc Al and hcp Ti. The calculated formation enthalpies are taken from Ref. 32, and were computed using VASP with similar settings as employed in the current work. Note that the formation entropies listed in this table are computed using force constants out to third neighbor, rather than first neighbor.

A comparison of the measured formation entropy with the current calculated value, indicated by the label "3NN harmonic," for $Al_3Ti$ shows a discrepancy of approximately $0.27k_B$/atom, with the measured value being more negative. In comparing experiment with the current calculations, it is important to note that our computed values were derived as the high-temperature limit of the vibrational entropy within the harmonic approximation, neglecting quasiharmonic, electronic and configurational contributions. The latter is expected to be small for the highly ordered intermetallic compounds in Al-Ti. Additionally, we found that the electronic contributions to the formation entropy were negligible [$-0.016k_B$ and $0.025k_B$ for $Al_3Ti$ ($DO_{22}$) and AlTi ($L1_0$), respectively]. The quasiharmonic corrections, however, were

found to be sizable. The last row of Table V represents results derived within the quasiharmonic approximation, and a comparison with the values listed in the row above shows that anharmonic effects give rise to an approximately $0.2k_B$/atom lowering of the vibrational formation entropy for both the $Al_3Ti$ and AlTi compounds at temperatures of 850 and 973 K, respectively. These sizeable corrections are seen to lead to significant improvement with measurements for the $Al_3Ti$ phase. A comparison of the quasi-harmonic-calculated formation free energies show good agreement with measurements for both compounds, with discrepancies between experiment and theory on the order of 20 meV/atom. This level of discrepancy between experiment and theory is also apparent in the enthalpies of formation, demonstrating relatively high accuracy in the current calculations of the formation entropies, provided quasiharmonic corrections are accounted for.

A particularly interesting aspect of the results shown in Fig. 6 is the large configurational dependencies of the vibrational mixing entropies displayed for each of the three Al-*TM* systems. Specifically, the effect of ordering on $S_{\mathrm{vib}}$ can be measured in terms of the ordering entropy, i.e., the magnitude of the difference between the vibrational entropies for disordered alloys (solid line) versus the ordered compounds (symbols). The magnitude of the ordering entropies in the Al-*TM* systems are seen to be significant, on the order of $0.2-0.3k_B$/atom, a value that represents a substantial fraction of the maximum possible configurational entropy difference ($0.69k_B$/atom for an alloy with a *TM* concentration of 0.5, or $0.56k_B$/atom for a concentration of 0.25 or 0.75). In a recent study[14] it was shown that ordering entropies of this magnitude are sufficient to lead to a several hundred degree reduction in the calculated order-disorder transition temperatures for hcp-based Ti-Al alloys. For fcc-based Al-*TM* alloys order-disorder transitions are not experimentally observed under equilibrium conditions, since fcc-based compounds generally melt prior to disordering. However, the substantial concentration and configuration dependencies of the vibrational entropies in these systems are expected to be strongly reflected in the calculated solvus boundaries. In calculations for the related Al-Sc system[15] vibrational contributions were found to lead to a substantial lowering, by several hundred K, of the calculated solvus boundary temperatures. Very similar results were obtained recently by Ravi *et al.* in their calculations of stable and metastable solubility limits in the Al-Cu system.[17] By making use of the TFC parametrization developed for Al-*TM* (*TM*=Ti, Zr, Hf) in the present work, we have estimated comparable reductions in the solvus-boundary temperatures for these systems as well;[43] these findings will be discussed in detail in a forthcoming publication. We note that the strong effect of vibrational entropy on calculated solvus boundaries was suggested over 50 years ago by Zener[55] based on an analysis of measured solubility data for Ni, Mn, Cr, Si, and Zr solutes in Al. The analysis suggests that substantial temperature shifts in calculated solvus boundaries are a relatively general feature of Al-*TM* systems. These findings and those of the most recent first-principles calculations[14,15,17] provide considerable motivation for developing efficient methods for computing vibrational contributions to free energies in the modeling of Al-*TM* alloy systems.

## V. CONCLUSIONS

The TFC approach has been applied as a framework for first-principles calculations of the vibrational thermodynamic properties of fcc-based Al-*TM* (*TM*=Ti, Zr, and Hf) alloys. In order to improve the efficiency of the vibrational entropy computations, we extended the transferable force constant approach[12,29,30] to these systems, finding it essential to account for the concentration dependence as well as bond length in the parametrization of bond force constants. Our calculations show for those structures involved in the fit, the TFC can reproduce the calculated vibrational entropies to within $0.10k_B$/atom, while for structures which are not included in the fit, the $\Delta S_{\mathrm{vib}}$ difference between the TFC results and direct calculations is about $0.11k_B$/atom. These errors associated with the application of the TFC approach to Al-*TM* (*TM*=Ti, Zr, and Hf) systems are, generally, about 20% of the overall magnitude of the vibrational entropy of mixing. The TFC method provides a highly efficient approach to calculating vibrational entropies when errors on this order are acceptable.

The magnitudes of the vibrational mixing entropies for ordered and disordered alloy configurations in the Al-*TM* (*TM*=Ti, Zr, and Hf) are calculated to be large and negative, with magnitudes (for ordered alloys) as large as $1.0k_B$/atom, in agreement with experimental measurements for the Al-Ti system. The vibrational entropy of ordering (defined as the difference in $S_{\mathrm{vib}}$ between ordered and disordered alloys with the same composition) is calculated to be on the order of $0.2-0.3k_B$/atom for concentrated alloy compositions. Previous work[14] has established the significance of these configurational dependencies of the vibrational entropy in the calculation of order-disorder transition temperatures in the Al-Ti system. Overall, the present and previous work related to phase stability establishes the significant role of vibrational entropy in governing the thermal stability of Al alloys with early transition metals.

## ACKNOWLEDGMENTS

This work was supported by the U.S. Department of Energy, Office of Basic Energy Science, under Contracts No. DE-FG02-02ER45997 (J.Z.L. and G.G.) and No. DE-FG02-01ER45910 (A.v.d.W. and M.A.). Supercomputing resources were provided by the National Partnership for Advanced Computational Infrastructure at the University of Illinois at Urbana-Champaign.

## APPENDIX: DESCRIPTIONS OF THE ORDERED STRUCTURES

Structural details for the twenty-three compounds listed in Table II are summarized in Table VI.

TABLE VI. Lattice constants, space group, and atomic Wyckoff positions of the twenty three ordered structures considered in the vibrational-entropy calculations used to construct the transferable-force-constant fits. In the last two columns, the lattice parameters ($a$, $b$, and $c$) and unit-cell angles ($\alpha$, $\beta$, and $\gamma$) are listed in consecutive rows.

| Structure | Space group (No.) | Wyckoff position | $x$ | $y$ | $z$ | $a/b/c$(Å) | $\alpha/\beta/\gamma$ |
|---|---|---|---|---|---|---|---|
| $Al_3Ti$ ($L1_2$) | $Pm\bar{3}m$ (221) | 3$c$ (Al) | 0.0000 | 0.5000 | 0.5000 | 3.9783 | |
| | | 1$a$ (Ti) | 0.0000 | 0.0000 | 0.0000 | | |
| $Al_3Ti$ ($D0_{22}$) | $I4/mmm$ (139) | 2$b$ (Al) | 0.0000 | 0.5000 | 0.5000 | 3.8441 | |
| | | 4$d$ (Al) | 0.0000 | 0.5000 | 0.2500 | 3.8441 | |
| | | 2$a$ (Ti) | 0.0000 | 0.0000 | 0.0000 | 8.6287 | |
| $Al_3Ti$ ($D0_{23}$) | $I4/mmm$ (139) | 4$c$ (Al) | 0.5000 | 0.0000 | 0.0000 | 3.8956 | |
| | | 4$d$ (Al) | 0.0000 | 0.5000 | 0.2500 | 3.8956 | |
| | | 4$e$ (Al) | 0.0000 | 0.0000 | 0.6248 | 16.6765 | |
| | | 4$e$ (Ti) | 0.0000 | 0.0000 | 0.1188 | | |
| $Al_2Ti$ | $Cmmm$ (65) | 2$a$ (Al) | 0.0000 | 0.0000 | 0.0000 | 12.1592 | |
| | | 2$c$ (Al) | 0.5000 | 0.0000 | 0.5000 | 3.9408 | |
| | | 4$g$ (Al) | 0.6728 | 0.0000 | 0.0000 | 3.9953 | |
| | | 4$h$ (Ti) | 0.1557 | 0.0000 | 0.5000 | | |
| AlTi ($L1_0$) | $P4/mmm$ (123) | 1$d$ (Al) | 0.5000 | 0.5000 | 0.5000 | 2.8154 | |
| | | 1$a$ (Ti) | 0.0000 | 0.0000 | 0.0000 | 2.8154 | |
| | | | | | | 4.0857 | |
| $AlTi_3$ ($L1_2$) | $Pm\bar{3}m$ (221) | 1$a$ (Al) | 0.0000 | 0.0000 | 0.0000 | 4.0435 | |
| | | 3$c$ (Ti) | 0.0000 | 0.5000 | 0.5000 | | |
| $Al_5Ti_3$ | $Cmmm$ (65) | 2$a$ (Al) | 0.0000 | 0.0000 | 0.0000 | 7.9646 | |
| | | 4$e$ (Al) | 0.2500 | 0.7500 | 0.0000 | 8.2429 | |
| | | 4$j$ (Al) | 0.5000 | 0.2424 | 0.5000 | 3.9080 | |
| | | 2$b$ (Ti) | 0.5000 | 0.0000 | 0.0000 | | |
| | | 4$h$ (Ti) | 0.2427 | 0.0000 | 0.5000 | | |
| $Al_3Ti_5$ | $Cmmm$ (65) | 2$b$ (Al) | 0.5000 | 0.0000 | 0.0000 | 7.8573 | |
| | | 4$h$ (Al) | 0.2586 | 0.0000 | 0.5000 | 8.3005 | |
| | | 2$a$ (Ti) | 0.0000 | 0.0000 | 0.0000 | 4.0127 | |
| | | 4$e$ (Ti) | 0.2500 | 0.7500 | 0.0000 | | |
| | | 4$j$ (Ti) | 0.5000 | 0.2662 | 0.5000 | | |
| $Al_3Zr$ ($L1_2$) | $Pm\bar{3}m$ (221) | 3$c$ (Al) | 0.5000 | 0.0000 | 0.5000 | 4.0965 | |
| | | 1$a$ (Zr) | 0.0000 | 0.0000 | 0.0000 | | |
| $Al_3Zr$ ($D0_{22}$) | $I4/mmm$ (139) | 2$a$ (Al) | 0.0000 | 0.0000 | 0.0000 | 3.9503 | |
| | | 4$d$ (Al) | 0.5000 | 0.0000 | 0.2500 | 3.9503 | |
| | | 2$b$ (Zr) | 0.0000 | 0.0000 | 0.5000 | 9.0181 | |
| Al3Zr ($D023$) | $I4/mmm$ (139) | 4$c$ (Al) | 0.5000 | 0.0000 | 0.0000 | 4.0076 | |
| | | 4$d$ (Al) | 0.0000 | 0.5000 | 0.2500 | 4.0076 | |
| | | 4$e$ (Al) | 0.0000 | 0.0000 | 0.3750 | 17.3019 | |
| | | 4$e$ (Zr) | 0.0000 | 0.0000 | 0.1185 | | |
| $Al_2Zr$ | $Cmmm$ (65) | 2$a$ (Al) | 0.0000 | 0.0000 | 0.0000 | 12.7914 | |
| | | 2$c$ (Al) | 0.5000 | 0.0000 | 0.5000 | 4.0650 | |
| | | 4$g$ (Al) | 0.3271 | 0.0000 | 0.0000 | 4.1561 | |
| | | 4$h$ (Zr) | 0.1528 | 0.0000 | 0.5000 | | |

TABLE VI. (*Continued.*)

| Structure | Space group (No.) | Wyckoff position | $x$ | $y$ | $z$ | $a/b/c$(Å) | $\alpha/\beta/\gamma$ |
|---|---|---|---|---|---|---|---|
| AlZr ($L1_0$) | $P4/mmm$ (123) | 1*d* (Al) | 0.5000 | 0.5000 | 0.5000 | 3.0298 | |
| | | 1*a* (Zr) | 0.0000 | 0.0000 | 0.0000 | 3.0298 | |
| | | | | | | 4.1677 | |
| $AlZr_3$ ($L1_2$) | $Pm\bar{3}m$ (221) | 1*a* (Al) | 0.0000 | 0.0000 | 0.0000 | 4.3576 | |
| | | 3*c* (Zr) | 0.5000 | 0.0000 | 0.5000 | | |
| $Al_5Zr_3$ | $Pmmm$ (47) | 1*a* (Al) | 0.0000 | 0.0000 | 0.0000 | 4.1902 | |
| | | 1*d* (Al) | 0.0000 | 0.5000 | 0.0000 | 8.5919 | |
| | | 1*e* (Al) | 0.5000 | 0.0000 | 0.5000 | 4.1902 | |
| | | 2*o* (Al) | 0.5000 | 0.2552 | 0.0000 | | |
| | | 1*h* (Zr) | 0.5000 | 0.5000 | 0.5000 | | |
| | | 2*n* (Zr) | 0.0000 | 0.2280 | 0.5000 | | |
| $Al_3Zr_5$ | $I4/mmm$ (139) | 2*b* (Al) | 0.0000 | 0.0000 | 0.5000 | 4.3328 | |
| | | 4*e* (Al) | 0.0000 | 0.0000 | 0.2492 | 4.3328 | |
| | | 2*a* (Zr) | 0.0000 | 0.0000 | 0.0000 | 16.9494 | |
| | | 8*g* (Zr) | 0.0000 | 0.5000 | 0.1294 | | |
| $Al_3Hf$ ($L1_2$) | $Pm\bar{3}m$ (221) | 3*c* (Al) | 0.5000 | 0.0000 | 0.5000 | 4.0815 | |
| | | 1*a* (Hf) | 0.0000 | 0.0000 | 0.0000 | | |
| $Al_3Hf$ ($D0_{22}$) | $I4/mmm$ (139) | 2*b* (Al) | 0.0000 | 0.0000 | 0.5000 | 3.9353 | |
| | | 4*d* (Al) | 0.0000 | 0.5000 | 0.2500 | 3.9353 | |
| | | 2*a* (Hf) | 0.0000 | 0.0000 | 0.0000 | 8.9098 | |
| $Al_3Hf$ ($D0_{23}$) | $I4/mmm$ (139) | 4*c* (Al) | 0.0000 | 0.5000 | 0.0000 | 3.9919 | |
| | | 4*d* (Al) | 0.5000 | 0.0000 | 0.2500 | 3.9919 | |
| | | 4*e* (Al) | 0.0000 | 0.0000 | 0.1246 | 17.1689 | |
| | | 4*e* (Hf) | 0.0000 | 0.0000 | 0.3808 | | |
| AlHf ($L1_0$) | $P4/mmm$ (123) | 1*d* (Al) | 0.5000 | 0.5000 | 0.5000 | 2.9824 | |
| | | 1*a* (Hf) | 0.0000 | 0.0000 | 0.0000 | 2.9824 | |
| | | | | | | 4.1967 | |
| $AlHf_3$ ($L1_2$) | $Pm\bar{3}m$ (221) | 1*a* (Al) | 0.0000 | 0.0000 | 0.0000 | 4.3128 | |
| | | 3*c* (Hf) | 0.5000 | 0.0000 | 0.5000 | | |
| $Al_5Hf_3$ | $P1$ (1) | 1*a* (Al) | 0.0078 | 0.0000 | 0.0000 | 8.5017 | 90.0000 |
| | | 1*a* (Al) | 0.5078 | 0.0000 | 0.0000 | 4.1813 | 102.7604 |
| | | 1*a* (Al) | 0.2500 | 0.5000 | 0.0000 | 4.0402 | 77.2396 |
| | | 1*a* (Hf) | 0.2500 | 0.0000 | 0.5000 | | |
| | | 1*a* (Hf) | 0.7500 | 0.0000 | 0.5000 | | |
| | | 1*a* (Hf) | 0.7500 | 0.5000 | 0.0000 | | |
| | | 1*a* (Hf) | 0.0200 | 0.5000 | 0.5000 | | |
| | | 1*a* (Hf) | 0.4800 | 0.5000 | 0.5000 | | |
| $Al_3Hf_5$ | $P4/mmm$ (123) | 1*a* (Al) | 0.0000 | 0.0000 | 0.0000 | 4.2662 | |
| | | 1*b* (Al) | 0.0000 | 0.0000 | 0.5000 | 4.2662 | |
| | | 1*c* (Al) | 0.5000 | 0.5000 | 0.0000 | 8.5133 | |
| | | 1*d* (Hf) | 0.5000 | 0.5000 | 0.5000 | | |
| | | 4*i* (Hf) | 0.5000 | 0.0000 | 0.2418 | | |

*Present address: National Renewable Energy Laboratory, Golden, Colorado 80401, USA.
[1] L. Anthony, J. K. Okamoto, and B. Fultz, Phys. Rev. Lett. **70**, 1128 (1993).
[2] L. Anthony, L. J. Nagel, J. K. Okamoto, and B. Fultz, Phys. Rev. Lett. **73**, 3034 (1994).
[3] B. Fultz, L. Anthony, L. J. Nagel, R. M. Nicklow, and S. Spooner, Phys. Rev. B **52**, 3315 (1995).
[4] L. J. Nagel, L. Anthony, and B. Fultz, Philos. Mag. Lett. **72**, 421 (1995).
[5] M. E. Manley and B. Fultz, Philos. Mag. B **80**, 1167 (2000).
[6] M. E. Manley, R. J. McQueeney, J. L. Robertson, B. Fultz, and D. A. Neumann, Philos. Mag. Lett. **80**, 591 (2000).
[7] O. Delaire, M. Kresch, and B. Fultz, Philos. Mag. **85**, 3567 (2005).
[8] T. L. Swan-Wood, O. Delaire, and B. Fultz, Phys. Rev. B **72**, 024305 (2005).
[9] P. D. Bogdanoff, T. L. Swan-Wood, and B. Fultz, Phys. Rev. B **68**, 014301 (2003).
[10] M. E. Manley, R. J. McQueeney, B. Fultz, R. Osborn, G. H. Kwei, and P. D. Bogdanoff, Phys. Rev. B **65**, 144111 (2002).
[11] P. D. Bogdanoff and B. Fultz, Philos. Mag. B **81**, 299 (2001).
[12] A. van de Walle and G. Ceder, Rev. Mod. Phys. **74**, 11 (2002).
[13] V. Ozolins, C. Wolverton, and A. Zunger, Phys. Rev. B **58**, R5897(1998).
[14] A. van de Walle, G. Ghosh, and M. Asta, in *Applied Computational Materials Modeling: Theory, Simulation and Experiment*, edited by G. Bozzolo, R. D. Noebe, and P. Abel (Springer, New York, 2007), p. 1.
[15] V. Ozolins and M. Asta, Phys. Rev. Lett. **86**, 448 (2001).
[16] V. Ozolins, B. Sadigh, and M. Asta, J. Phys.: Condens. Matter **17**, 2197 (2005).
[17] C. Ravi, C. Wolverton, and V. Ozolins, Europhys. Lett. **73**, 719 (2006).
[18] J. M. Sanchez, F. Ducastelle, and D. Gratias, Physica A **128**, 334 (1984).
[19] A. van de Walle and M. Asta, in *Handbook of Materials Modeling*, edited by S. Yip (Springer, The Netherlands, Dordrecht, 2005).
[20] J. W. D. Connolly and A. R. Williams, Phys. Rev. B **27**, 5169 (1983).
[21] D. de Fontaine, Solid State Phys. **47**, 33 (1994).
[22] A. A. Maradudin, in *Dynamical Properties of Solids*, edited by G. K. Horton and A. A. Maradudin (North-Holland, Amsterdam, 1974), p. 3.
[23] A. A. Maradudin, *Theory of Lattice Dynamics in the Harmonic Approximation* (Academic Press, New York, 1971).
[24] N. W. Ashcroft and N. D. Mermin, *Solid State Physics* (Holt Rinehart and Winston, New York, 1976).
[25] M. Sluiter and Y. Kawazoe, Philos. Mag. A **78**, 1353 (1998).
[26] M. H. F. Sluiter, M. Weinert, and Y. Kawazoe, Phys. Rev. B **59**, 4100 (1999).
[27] Ph. Ghosez, E. Cockayne, U. V. Waghmare, and K. M. Rabe, Phys. Rev. B **60**, 836 (1999).
[28] P. Giannozzi, S. de Gironcoli, P. Pavone, and S. Baroni, Phys. Rev. B **43**, 7231 (1991).
[29] A. van de Walle and G. Ceder, Phys. Rev. B **61**, 5972 (2000).
[30] A. van de Walle, Ph.D. thesis, Massachusetts Institute of Technology, Cambridge, 2000.
[31] E. J. Wu, G. Ceder, and A. van de Walle, Phys. Rev. B **67**, 134103 (2003).
[32] G. Ghosh and M. Asta, Acta Mater. **53**, 3225 (2005).
[33] A. van de Walle, G. Ceder, and M. Asta, CALPHAD: Comput. Coupling Phase Diagrams Thermochem. **26**, 491 (2002).
[34] G. Kresse and J. Hafner, Phys. Rev. B **47**, 558 (1993).
[35] G. Kresse and J. Hafner, J. Phys.: Condens. Matter **6**, 8245 (1994).
[36] J. P. Perdew, J. A. Chevary, S. H. Vosko, K. A. Jackson, M. R. Pederson, D. J. Singh, and C. Fiolhais, Phys. Rev. B **46**, 6671 (1992).
[37] H. J. Monkhorst and J. D. Pack, Phys. Rev. B **13**, 5188 (1976).
[38] M. Methfessel and A. T. Paxton, Phys. Rev. B **40**, 3616 (1989).
[39] D. Singh and R. P. S. Rathore, Phys. Status Solidi B **170**, 443 (1992).
[40] I. Akgun and G. Ugur, Phys. Rev. B **51**, 3458 (1995).
[41] A. van de Walle and G. Ceder, J. Phase Equilib. **23**, 348 (2002).
[42] E. Clouet, J. M. Sanchez, and C. Sigli, Phys. Rev. B **65**, 094105 (2002).
[43] Z. Liu, Ph.D. thesis, Northwestern University, Evanston, IL, 2006.
[44] J. Zou and C. L. Fu, Phys. Rev. B **51**, 2115 (1995).
[45] G. Ghosh, S. Delsante, G. Borzone, M. Asta, and R. Ferro, Acta Mater. **54**, 4977 (2006).
[46] G. Ghosh (unpublished).
[47] O. Kubaschewski and W. A. Dench, Acta Metall. **3**, 339 (1955).
[48] O. Kubaschewski and G. Heymer, Trans. Faraday Soc. **56**, 473 (1960).
[49] S. Z. Meschel and O. J. Kleppa, *Metallic Alloys: Experimental and Theoretical Perspectives*, in NATO ASI Series E: Applied Sciences, Vol. 256, edited by J. S. Faulkner and R. G. Jordan (Plenum, New York, 1994), p. 103.
[50] M. Nassik, F. Z. Chrifi-Alaoui, K. Mahdouk, and J. C. Gachon, J. Alloys Compd. **350**, 151 (2003).
[51] V. V. Samokhval, P. A. Poleshchuk, and A. A. Vecher, Russ. J. Phys. Chem. **45**, 1174 (1971).
[52] R. G. Reddy, A. M. Yahya, and L. Brewer, J. Alloys Compd. **321**, 223 (2001).
[53] P. D. Desai, J. Phys. Chem. Ref. Data **16**, 109 (1987).
[54] C. Triguero, M. Porta, and A. Planes, Phys. Rev. B **73**, 054401 (2006).
[55] C. Zener, in *Thermodynamics in Physical Metallurgy*, edited by C. Zener (ASM, Cleveland, OH, 1950), pp. 16–27.